

Modular Design of Domain Assembly in Porous Coordination Polymer Crystals via Reactivity-Directed Crystallization Process

Tomohiro Fukushima,[†] Satoshi Horike,^{†,‡} Hirokazu Kobayashi,[§] Masahiko Tsujimoto,[§] Seiji Isoda,[§] Maw Lin Foo,^{§,||} Yoshiaki Kubota,[#] Masaki Takata,[¶] and Susumu Kitagawa^{*,†,§,||}

[†]Department of Synthetic Chemistry and Biological Chemistry, Graduate School of Engineering, Kyoto University, Katsura, Nishikyo-ku, Kyoto 615-8510, Japan

[‡]PRESTO, Japan Science and Technology Agency, 4-1-8 Honcho, Kawaguchi, Saitama 332-0012, Japan

[§]Institute for Integrated Cell-Material Sciences (WPI-iCeMS), Kyoto University, Yoshida, Sakyo-ku, Kyoto 606-8501, Japan

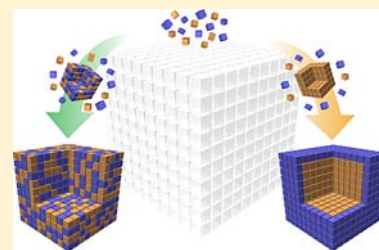
^{||}ERATO Kitagawa Integrated Pores Project, Japan Science and Technology Agency, Kyoto Research Park Bldg #3, Shimogyo-ku, Kyoto 600-8815, Japan

[#]Department of Physical Science, Graduate School of Science, Osaka Prefecture University, Osaka, 599-8531, Japan

[¶]RIKEN SPring-8 Center, Kouto, Sayo-cho, Sayo-gun, Hyogo 679-5198, Japan

Supporting Information

ABSTRACT: The mesoscale design of domain assembly is crucial for controlling the bulk properties of solids. Herein, we propose a modular design of domain assembly in porous coordination polymer crystals via exquisite control of the kinetics of the crystal formation process. Employing precursors of comparable chemical reactivity affords the preparation of homogeneous solid-solution type crystals. Employing precursors of distinct chemical reactivity affords the preparation of heterogeneous phase separated crystals. We have utilized this reactivity-directed crystallization process for the facile synthesis of mesoscale architecture which are either solid-solution or phase-separated type crystals. This approach can be also adapted to ternary phase-separated type crystals from one-pot reaction. Phase-separated type frameworks possess unique gas adsorption properties that are not observed in single-phasic compounds. The results shed light on the importance of crystal formation kinetics for control of mesoscale domains in order to create porous solids with unique cooperative functionality.



INTRODUCTION

The nanoscale design of porous solids is crucial for imparting functionality,¹ and many different ions/molecules have been employed as modules to achieve such purpose. On the other hand, besides the nanoscale regime, one can employ chemistry at the mesoscale regime as well for design of adsorptive properties. As these solids consist of a statistical ensemble of molecules, interactive communication between mesoscale domains is crucial in determining bulk properties² such as magnetism,³ ion transport,⁴ and phase transitions.⁵ Hence, it is expected that the rational design of porous solids in the mesoscale regime could unveil a plethora of cooperative, on-demand, or multifunctional adsorptive systems.

Porous coordination polymers (PCPs), also known as metal–organic frameworks (MOFs), are good candidates due to their synthetic flexibility⁶ and structural and functional diversity.⁷ Due to the inherent structural designability of PCP synthesis, we can expect the combination of suitable modules will enable us to control the number, size, shape, and position of the mesoscale domain modules in PCP/MOF crystals (Scheme 1). The inherent advantage of this approach is to introduce rational structural and functional chemistry to mesoscopic science, which has been thus far difficult to achieve in synthetic materials chemistry. Based on this motivation,

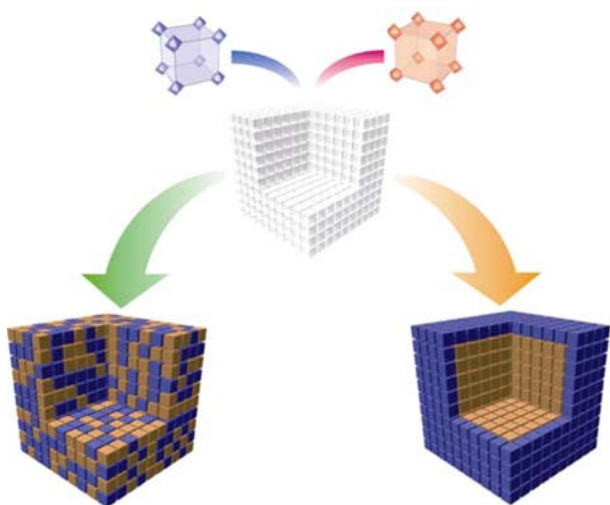
there has been some previous attempts to control the domain assembly in PCP/MOF crystals.⁸ Employing one-pot reaction affords the preparation of solid-solution type frameworks that contain a stochastic mixture of domains to form a homogeneous distribution in a crystal⁹ and employing sequential reaction affords the preparation of phase-separated type frameworks that contain macroscopic-sized domains as blocks, layered, or core/shell fashion to form a heterogeneous distribution in a crystal.¹⁰ However, at present, a straightforward synthetic methodology for mesoscale design has not yet been established.

Here, we describe a simple and robust synthetic methodology to design modular domain assembly by rationally exploiting the kinetic aspects of PCP/MOF crystallization. As coordination bonds have a reversible and dynamic bonding nature, the difference in the chemical reactivity of the precursors directs the crystal formation kinetics of PCP/MOFs.¹¹ Regulation of the temporal crystal formation process allows the control of modular domain assembly in PCP/MOFs, binary solid-solution, binary phase-separated type crystals, and even ternary phase-separated type crystals from a one-pot

Received: April 14, 2012

Published: July 20, 2012

Scheme 1. Schematic Illustration of the Construction of PCP Crystals from Binary Crystal Domain Modules^a



^aThe modular design of the domain assembly in the PCP crystals allows the mesoscale structural chemistry, represented by (i) solid-solution type compounds with a stochastic distribution (left), and (ii) phase-separated type compounds with ordered distribution (right). The size, shape, and distribution of the domain module can be modified to control the porous properties.

reaction. Consequently, the cooperativity of the adsorption properties is influenced by the spatial domain arrangement of crystals despite having identical molecular formula. We thus propose the concept that the modular design of domain assembly in porous materials influences the porous properties via communication between mesoscale domains.

RESULTS AND DISCUSSION

Porous coordination polymers with a two-dimensional (2D) interdigitated layer structure (a coordination polymer with an interdigitated structure, denoted as CID) were utilized as a structural platform for the fabrication of PCP/MOFs. The frameworks can be rationally realized as being a common framework,^{9d,12} even when different metal ions are employed. Pseudo-octahedral coordination geometry in CID type framework prevents the formation of a distinct phase from the mixed-component reaction.¹³ In this study, we employed $\{[M(\text{NO}_2\text{-ip})(\text{bpy})]0.5\text{DMF}\cdot 0.5\text{MeOH}\}_n$ (MCID-5DG, where $M = \text{Zn, Mn, and Ni}$, and $\text{NO}_2\text{-ip} = 5\text{-nitroisophthalate}$ and $\text{bpy} = 4,4'\text{-bipyridyl}$). We synthesized isostructures with different metal ions, and both crystal structures (ZnCID-5DG and MnCID-5DG, where G is guest molecule) are shown in Figure 1.

We utilized the difference in the chemical reactivity of the precursors to control the crystal formation kinetics. The crystal formation processes of the PCP/MOFs were defined by two consecutive processes: (i) the formation of nuclei (i.e., a nucleation process), and (ii) the growth of nuclei to form crystals (i.e., a growth process).¹⁴ The reaction solutions are transparent during the induction period (t_{ind}), and powders are gradually obtained through the nucleation and growth processes as the reaction proceeds. In this regard, the difference in the chemical reactivity of the precursors directs both the nucleation and growth processes, and consequently influences the induction time (t_{ind}) on the macroscopic scale.

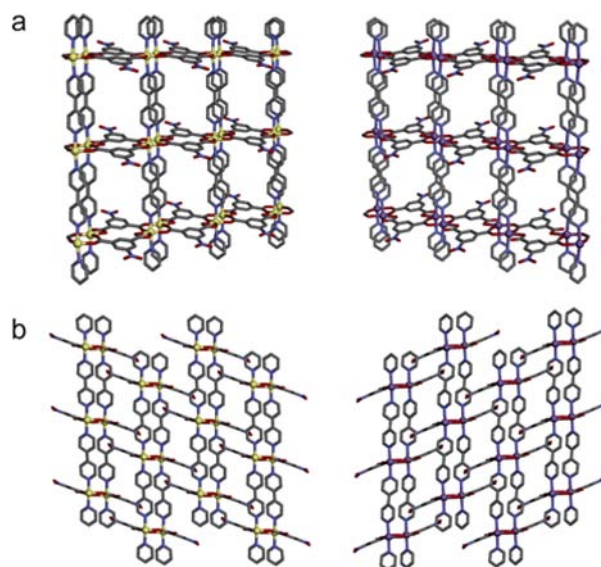


Figure 1. (a) Two-dimensional layer structure of ZnCID-5DG (left) and MnCID-5DG (right). (b) The assembled structure of ZnCID-5DG (left) and MnCID-5DG (right). Yellow, purple, red, blue, and gray represent Zn, Mn, O, N, and C atoms, respectively.

The crystal formation kinetics of the compounds was studied using a time-course analysis of the yields of reaction products. The reaction of the metal perchlorates and bpy with disodium-5-nitroisophthalate ($\text{Na}_2\text{NO}_2\text{-ip}$) or 5-nitroisophthalic acid ($\text{H}_2\text{NO}_2\text{-ip}$) were employed for different reaction conditions considering the different chemical reactivity of the precursors. Although the final products were identical regardless of the precursors used (see Supporting Information), the crystal formation kinetics was sensitive to the chemical reactivity of the precursors,¹¹ which depended particularly on the acidity of the precursors.¹⁵ When using $\text{Na}_2\text{NO}_2\text{-ip}$ as a precursor, the coordination reaction to form the framework was accelerated markedly, and this resulted in the rapid preparation of crystals. Owing to the high chemical reactivity of $\text{Na}_2\text{NO}_2\text{-ip}$, similar crystal formation kinetics was observed for both zinc and manganese perchlorate precursors (Figure 2a). In contrast, the

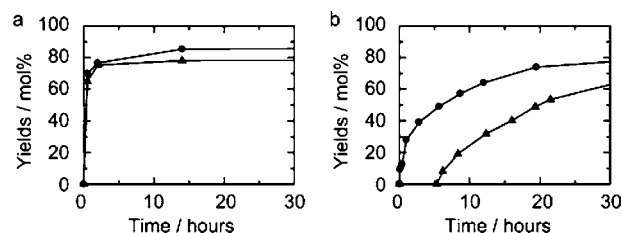


Figure 2. Time-course analysis of the crystal formation of ZnCID-5DG (circles) and MnCID-5DG (triangles) using: (a) $\text{Na}_2\text{NO}_2\text{-ip}$ and (b) $\text{H}_2\text{NO}_2\text{-ip}$ as precursors.

crystal formation process showed a different behavior employing 5-nitroisophthalic acid ($\text{H}_2\text{NO}_2\text{-ip}$) as a low-reactive precursor. In particular, the value of t_{ind} for crystal formation is highly dependent on the chemical reactivity of each metal ion. The reaction employing zinc perchlorate exhibited $t_{\text{ind}} = 100$ s, while the reaction employing manganese perchlorate exhibited $t_{\text{ind}} = 5.5$ h (Figure 2b). Hence, the reaction of metal ions with low-reactive precursor provided a clear difference in the crystal formation behavior.

One-Pot Synthesis of Metal-Based Solid-Solution Type PCPs. As we observed either comparable or distinct reactivity during the formation of crystals, we tried to fabricate binary metal-based solid-solution type crystals using high-reactivity conditions. We employed the one-pot reaction of $\text{Na}_2\text{NO}_2\text{-ip}$ and bpy with zinc and manganese perchlorate salts in DMF/MeOH at 70 °C for 3 days as high-reactivity conditions. The reactions yielded pale-yellow crystalline powders with a formula of $\{[\text{Zn}_{1-x}\text{Mn}_x(\text{NO}_2\text{-ip})(\text{bpy})](0.5\text{DMF}\cdot 0.5\text{MeOH})\}_n$, denoted as $\text{Zn}_{1-x}\text{Mn}_x\text{CID-5}\text{DG}$ (where x is the Mn content of the sample). X-ray powder diffraction (XRPD) data of the product were measured to elucidate the crystalline character of the $\text{Zn}_{1-x}\text{Mn}_x\text{CID-5}\text{DG}$ samples (Figure 3a). The powder pattern of $\text{Zn}_{1-x}\text{Mn}_x\text{CID-5}\text{DG}$

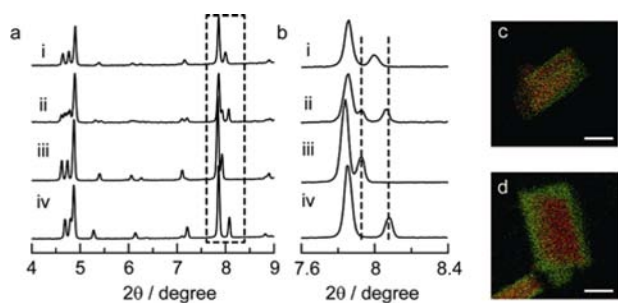


Figure 3. (a) XRPD data for (i) solid-solution type $\text{Zn}_{1-x}\text{Mn}_x\text{CID-5DG}$ ($x = 0.46$), (ii) phase-separated type Zn/MnCID-5DG ($x = 0.46$), and the parent pure compounds (iii) MnCID-5DG and (iv) ZnCID-5DG (wavelength = 0.8 Å). (b) Expansion of the data shown in part a from $2\theta = 7.6^\circ$ to 8.4° . (c) Overlapped image of elemental mapping for solid-solution type $\text{Zn}_{1-x}\text{Mn}_x\text{CID-5DG}$ (red, Zn; green Mn). The scale bar corresponds to 1 μm . (d) Overlapped image of elemental mapping for phase-separated type Zn/MnCID-5DG (red, Zn; green Mn). The scale bar corresponds to 1 μm .

5DG showed a single peak in the intermediate position between ZnCID-5DG and MnCID-5DG for $2\theta = 8.0^\circ$ (Figure 3b). This result indicates that the reaction product did not include the parent pure compounds, ZnCID-5DG and MnCID-5DG . LeBail analysis on the diffraction data indicated that $\text{Zn}_{1-x}\text{Mn}_x\text{CID-5DG}$ has intermediate cell parameters between ZnCID-5DG and MnCID-5DG (see Supporting Information), which exhibited the formation of a solid-solution type compound, according to Vegard's law.¹⁶ Scanning transmission electron microscopy–energy dispersive X-ray (STEM-EDX) measurements were conducted to check the distribution of metal species in the crystals, as shown in Figure 3c. STEM-EDX images of $\text{Zn}_{1-x}\text{Mn}_x\text{CID-5DG}$ revealed that both Zn and Mn were dispersed homogeneously in the crystals, which supports the proposed homogeneous distribution of each metal in the crystals.

We studied the time-dependent formation process of solid-solution type $\text{Zn}_{1-x}\text{Mn}_x\text{CID-5DG}$ using a time-course analysis (see Supporting Information). XRPD data for products with different reaction time showed similar powder patterns, and the crystals contained the same amount of Zn and Mn ions for each reaction time. The results indicate that both metal ions have a similar chemical reactivity when forming frameworks when $\text{Na}_2\text{NO}_2\text{-ip}$ was employed in a one-pot reaction, and both metal ions are dispersed statistically in the crystals to form a single crystalline solid-solution type framework.⁹ The key for the successful preparation of solid-solution type compounds is the

analogous behavior of both the crystal formation kinetics and lattice of the coordination frameworks.

One-Pot Synthesis of Metal-Based Phase-Separated Type PCPs. Analogous crystal formation kinetics of each component in the one-pot reactions produced a solid-solution type framework, whereas distinct crystal formation kinetics would influence the crystal formation behavior to obtain phase-separated type structural domains in a crystal. $\text{H}_2\text{NO}_2\text{-ip}$, as a low-reactive precursor, was selected for the successful preparation of phase-separated type crystals. The one-pot reaction of $\text{H}_2\text{NO}_2\text{-ip}$ and bpy with zinc and manganese perchlorate salts in a DMF/MeOH solution at 70 °C for 3 days produced pale-yellow crystalline powders $\{[\text{Zn}_{1-x}\text{Mn}_x(\text{NO}_2\text{-ip})(\text{bpy})](0.5\text{DMF}\cdot 0.5\text{MeOH})\}_n$, denoted as Zn/MnCID-5DG (where x is the Mn content in the sample). XRPD data were measured to elucidate the crystalline character of Zn/MnCID-5DG (Figure 3a,b). The resulting powder pattern showed two peaks occurring at $2\theta = 7.9^\circ$ and 8.1° , which were assigned to superimposition of the diffraction patterns of pure ZnCID-5DG and MnCID-5DG . Although these crystals were synthesized from a one-pot reaction, the solid-solution phase was not formed because of the different crystal formation kinetics. Meanwhile, there was the possibility of forming a mixture of ZnCID-5DG and MnCID-5DG . STEM-EDX measurements were conducted to evaluate the distribution of metal ions in the crystals of Zn/MnCID-5DG (Figure 3d). Observations on Zn/MnCID-5DG revealed that all the crystals contained Zn-rich inner crystals and Mn-rich outer crystals. Isolated pure ZnCID-5DG , MnCID-5DG , or solid-solution type compounds were not observed. These results demonstrated that synthesis of phase-separated type crystals of Zn/MnCID-5DG occurs via a bottom-up self-assembly process.

We studied the formation mechanism of phase-separated type crystals via a bottom-up self-assembly process. The nucleation process for phase-separated type compounds is discussed by observations of crystal size.^{14b,d} It is known that a rapid nucleation rate leads to high particle concentrations resulting in small particles. In contrast, a slow nucleation rate leads to a low concentration of seed, which consumes the monomer, resulting in larger particles. Owing to the clear difference in nucleation kinetics, the average size of the pure Mn compound particles was larger than that of the pure Zn compound particles (see Supporting Information). The size of the phase-separated type crystals was similar to the size of the pure Zn crystals, which suggests that the nucleation process of the phase-separated type compounds is dominated by the Zn-rich crystals. We also studied the nucleation and growth mechanisms of the Mn-rich crystals using a time-course analysis of the chemical composition of the crystals (see Supporting Information). The chemical composition of Zn/MnCID-5DG was rich in Zn during the initial reaction period, and thereafter the ratio of Mn in the crystals gradually increased. This tendency was supported by ex situ characterization data for the crystals using XRPD (see Supporting Information). Phase-separated type Zn/MnCID-5DG contained a Zn-rich crystalline phase during the initial reaction period, followed by the formation of a Mn-rich crystalline phase. Importantly, the formation of the Mn component in phase-separated type Zn/MnCID-5DG was faster than the formation of the pure Mn crystals (see Supporting Information). These results indicate that the presence of Zn-rich crystals influenced the crystal formation process of the Mn component from the heterogeneous nucleation of Mn-rich crystals on the Zn-rich crystals.

Clear differences in crystal formation kinetics of isostructural components promoted the formation of phase-separated type frameworks in the one-pot reaction.¹⁷

The reactivity-directed crystallization process is widely adopted for the facile fabrication of heterogeneous crystal systems. The synthesis of ternary phase-separated type crystals was demonstrated. The crystal formation kinetics for the construction of MCID-5 Δ G structures depends on the metal ion used (Zn^{2+} , Ni^{2+} , or Mn^{2+}) when using $\text{H}_2\text{NO}_2\text{-ip}$ as a low-reactive precursor. The reaction with zinc perchlorate occurred in a short period of time ($t_{\text{ind}} = 100$ s) and the reaction with nickel perchlorate occurred in a moderate period of time ($t_{\text{ind}} = 4.5$ h), while the reaction with manganese perchlorate occurred over a longer period of time ($t_{\text{ind}} = 5.5$ h). The crystal formation reactions with distinct kinetics afforded the preparation of binary phase-separated type Zn/NiCID-5 Δ G (see Supporting Information), and even ternary phase-separated type Zn/Ni/MnCID-5 Δ G crystals with good yields and purity, as shown in Figure 4. In the ternary system, the

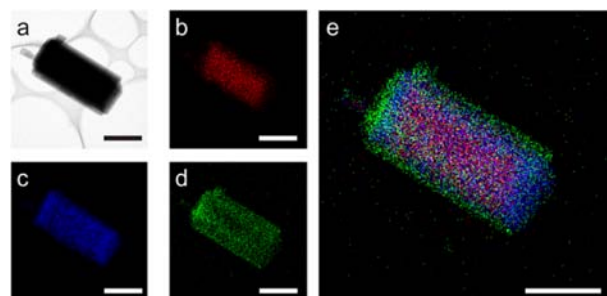


Figure 4. STEM-EDX images of the ternary phase separated compound of Zn/Ni/MnCID-5 Δ G: (a) TEM-images, (b) Zn-K, (c) Ni-K, (d) Mn-K elemental mapping images and (e) overlap image (red, Zn; blue, Ni; green, Mn). The scale bar corresponds to 2 μm .

formation of Zn/Ni phase-separated type crystals occurred, followed by the formation of Mn-rich crystals on the Zn/Ni phase-separated type crystals, and finally the Zn/Ni/Mn phase-separated type crystals formed.

Gas Sorption Behavior of Solid-Solution and Phase-Separated Type PCPs. It is of interest to investigate the difference in the porous properties of the solid-solution and phase-separated type compounds with the same chemical composition. Recently, PCP/MOFs with structural flexibility, which exhibit deformation or displacement behavior of framework upon gas accommodation, have been highlighted.¹⁸ The structural change of frameworks gives a unique sorption profile which is called gate-opening type gas sorption phenomena.¹⁹ These flexible frameworks change their structure from a closed (nonporous) form to an open (porous) form on gas accommodation. Consequently, the framework behaves as nonporous to gases in the initial state, and structural transformation from nonporous phase to porous phase at a given pressure (P_{go}) triggered a sudden rise in gas adsorption. Theoretical study indicates the importance of phase transition character of flexible PCP/MOFs driven by stabilization of guest adsorption.²⁰ As the gate-opening phenomena have the phase transition characteristics, cooperativity is great important factor to change the behavior regarding to either host-guest clathrate²¹ or structural transition of the host framework.²² Since modification of domain assembly in one crystal affects the

cooperativity of phase behavior through interactive communication of cells, the gate-opening gas sorption behavior can be controlled for adsorptive functions, such as gas storage and separation.

We investigated the gate-opening type sorption behavior for MCID-5 due to the structural change of frameworks (see Supporting Information). The adsorption isotherms of methanol at 298 K for pure ZnCID-5 and MnCID-5 are shown in Figure 5a. The total uptake for ZnCID-5 and

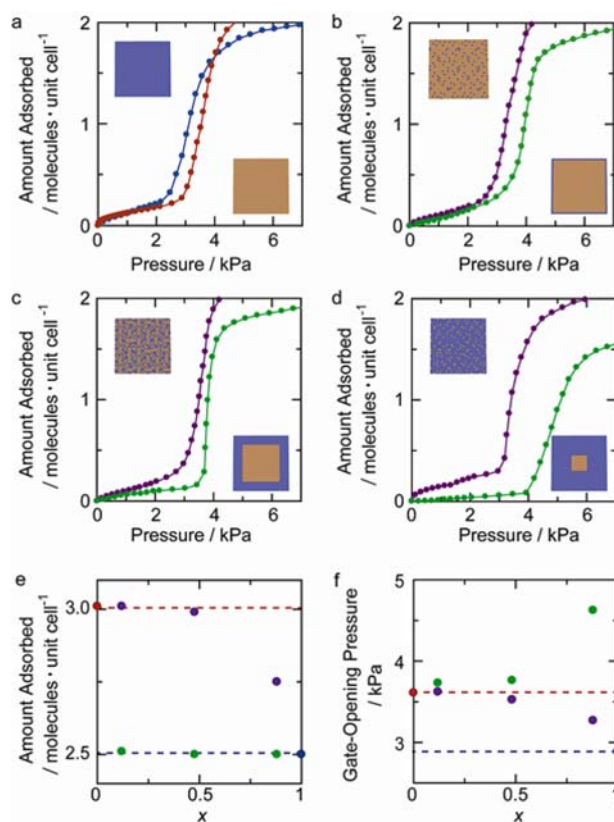


Figure 5. (a) Adsorption isotherm of methanol at 298 K for the pure parent compounds ZnCID-5 (orange) and MnCID-5 (blue) in the range 0–6 kPa. The adsorption isotherms of methanol at 298 K for solid-solution type $[\text{Zn}_{1-x}\text{Mn}_x(\text{NO}_2\text{-ip})(\text{bpy})]_n$ (purple) and phase-separated type $[\text{Zn}_{1-x}\text{Mn}_x(\text{NO}_2\text{-ip})(\text{bpy})]_n$ (green) for (b) $x = 0.12$, (c) $x = 0.46$, and (d) $x = 0.88$ in the range 0–6 kPa. Plots of (e) adsorption amount at $P = 16$ kPa,²³ and (f) the gate-opening pressure (P_{go}) for ZnCID-5 (orange), MnCID-5 (blue), solid-solution type frameworks (purple), and phase-separated type frameworks (green) as a function of the metal ratio (x) in the compounds.

MnCID-5 was 3 and 2.5 molecules/unit cell at $P = 16$ kPa,²³ respectively, and the value of P_{go} for ZnCID-5 and MnCID-5 was 3.71 and 2.93 kPa, respectively,²⁴ because of the difference in their structural flexibility (see Supporting Information). Parts b–d of Figure 5 show the adsorption isotherms of methanol for solid-solution and phase-separated type compounds $[\text{Zn}_{1-x}\text{Mn}_x(\text{NO}_2\text{-ip})(\text{bpy})]_n$ (where $x = 0.12, 0.46,$ and 0.88) that were prepared by reactivity-directed crystallization process (see Supporting Information). Although the solid-solution and phase-separated type compounds had the same formula, they showed distinct gate-opening sorption behavior. As shown in Figure 5e,f, solid-solution type $\text{Zn}_{1-x}\text{Mn}_x\text{CID-5}$ compounds have intermediate values for their total uptake and a value of P_{go} between that of ZnCID-5 and MnCID-5, which was dependent

on the metal ratio present. This tendency is consistent with previous report.^{9d}

In contrast, the phase-separated type frameworks exhibited anomalous sorption behaviors, which are not explained by a simple overlapping of the behavior of the two pure parent compounds. The phase-separated type frameworks exhibited a constant uptake (2.5 molecules/unit cell) at $P = 16$ kPa,²³ which was independent of the metal ratio in the framework, as shown in Figure 5e. Although the adsorption amount was lower than that of the pure Zn framework, the Mn domains dominated the adsorption amount in phase-separated type frameworks. This can be understood as follows. Because of the mutual integration of the Zn and Mn crystal domains in the phase-separated type compounds, the presence of Mn domains do not allow adsorbing the maximum uptake of the pure Zn framework (3.0 molecules/unit cell), otherwise the phase-separated type crystals would segregate. The constant uptake of the phase-separated type frameworks at $P = 16$ kPa²³ indicates that these crystals possess a strong coupling of Mn and Zn phases through their interfaces. In addition, the phase-separated type frameworks exhibited an anomalous gate-opening behavior. The value of P_{go} of the phase-separated type frameworks increased upon the increase of Mn ratio in the phase-separated type framework, which was even higher than the solid-solution type frameworks and the parent crystals, as shown in Figure 5f. Although the structure–property relationships for this sorption behavior have not been elucidated from the experimental point of view, there are suggestive works on the mechanism. Theoretical study suggests the importance of interplay of adsorption interaction and elastic deformation. Cooperative sorption behavior is investigated in case with the strong host–host interaction in elastic frameworks.²² One possible mechanism can be considered that mutual integration of two distinct phases in one crystal would enhance the elasticity of overall framework which leads to high cooperativity in sorption systems. We are still unsure why domain assembly in phase-separated type architecture enhances the cooperativity of gate-opening behavior, and we will explore this theme in our future work. However, there is some precedence in the nanowire literature: the elasticity of phase-separated Ge/Si semiconducting nanowires shows nonlinear relationships between mother compounds.²⁵ The coexistence of ordered domains in phase-separated architecture might enhance the elasticity of framework which leads to high cooperativity of gate-opening type sorption behavior. These results demonstrate the potential diversity of porous functions induced by the mesoscopic design of modular domain assembly in porous crystals.

CONCLUSIONS

In conclusion, we have proposed a simple methodology for the modular design of domain assembly in PCP/MOF crystals. This reactivity-directed crystallization process enables a bottom-up approach to be adopted for variable domain assembly, resulting in a facile preparation of PCP/MOF crystals, ranging from perfect homogeneity (solid solution) to heterogeneity (phase separation). Regulation of the reaction kinetics of frameworks is the key for the successful synthesis of domain-controlled porous coordination frameworks. The control of the domain distribution in a crystal is widely applicable via a self-assembly process, and we were able to fabricate binary solid-solution, binary phase-separated, and even ternary phase-separated systems using a one-pot reaction. We

also investigated how crystal domain assembly influenced the structural flexibility of the frameworks, and as a consequence, distinct sorption behavior was observed, regardless of the same chemical composition of compounds. Especially, phase-separated type compounds showed an anomalous cooperative gas sorption behavior that cannot be explained by a simple overlap of single-phasic crystals. These results demonstrate the potential diversity of porous functions contributed by the mesoscopic design of porous crystals. We believe that the modular design of domain assembly in porous solids opens up cooperative functionality in mesoscale science.

EXPERIMENTAL SECTION

Synthesis of Na₂NO₂-ip. H₂NO₂-ip (2.1 g, 10 mmol) and NaOH (0.8 g, 20 mmol) were dissolved in 40 mL of water and precipitated by the addition of 70 mL of ethanol. The white precipitate was filtered and dried at room temperature in vacuo to give 1.63 g (yield = 64%). Caution! Na₂NO₂-ip is explosive on heating.

Synthesis of {[M(NO₂-ip)(bpy)]0.5DMF-0.5MeOH}_n (M = Zn, Mn, and Ni). ZnCID-5CG, MnCID-5CG, and NiCID-5CG were synthesized according to a slightly modified published procedure.^{9d} Mn(ClO₄)₂·6H₂O (0.37 g, 1.0 mmol) and 5-nitroisophthalic acid (0.22 g, 1.0 mmol) were dissolved in 20 mL of *N,N'*-dimethylformamide (DMF). 4,4'-Bipyridyl (0.16 g 1.0 mmol) was dissolved in 20 mL of methanol. A solution of bpy in methanol was then slowly layered onto the reactant in the DMF solution. After a few days at 70 °C, colorless plate-like single crystals of MnCID-5CG were obtained. Caution! Metal perchlorate is explosive on heating.

Synthesis of Solid-Solution Type {[Zn_{1-x}Mn_x(NO₂-ip)(bpy)]0.5DMF-0.5MeOH}_n. Solid-solution type Zn_{1-x}Mn_xCID-5CG was synthesized as follows. Disodium-5-nitroisophthalate (0.26 g, 0.10 mmol) and 4,4'-bipyridyl (0.16 g, 1.0 mmol) were dissolved in 40 mL of 1:1 v:v DMF/MeOH solution at 70 °C. Zn(ClO₄)₂·6H₂O (0.18 g, 0.5 mmol) and Mn(ClO₄)₂·6H₂O (0.18 g, 0.5 mmol) were then added to the solution under stirring. After a few days, pale-yellow crystalline powders of solid-solution type Zn_{1-x}Mn_xCID-5CG were obtained.

Synthesis of Phase-Separated Type {[Zn_{1-x}Mn_x(NO₂-ip)(bpy)]0.5DMF-0.5MeOH}_n. Phase-separated Zn/MnCID-5CG was synthesized as follows. 5-Nitroisophthalic acid (0.21 g, 0.10 mmol) and 4,4'-bipyridyl (0.16 g, 1.0 mmol) were dissolved in 40 mL of 1:1 v:v DMF/MeOH solution at 70 °C. Zn(ClO₄)₂·6H₂O (0.18 g, 0.5 mmol) and Mn(ClO₄)₂·6H₂O (0.18 g, 0.5 mmol) were then added to the solution under stirring. After a few days, pale-yellow crystalline powders of phase-separation type Zn/MnCID-5CG were obtained.

Synthesis of Ternary Phase-Separated Type {[Zn_{1-x-y}Ni_xMn_y(NO₂-ip)(bpy)]0.5DMF-0.5MeOH}_n. Ternary phase-separated Zn/Ni/MnCID-5CG was synthesized as follows. 5-Nitroisophthalic acid (0.25 g, 0.10 mmol) and 4,4'-bipyridyl (0.16 g, 1.0 mmol) were dissolved in 40 mL of 1:1 v:v DMF/MeOH solution at 70 °C. Zn(ClO₄)₂·6H₂O (0.12 g, 0.3 mmol), Ni(ClO₄)₂·6H₂O (0.12 g, 0.3 mmol) and Mn(ClO₄)₂·6H₂O (0.12 g, 0.3 mmol) were then added to the solution under stirring. After a few days, pale-green crystalline powders of ternary phase-separated Zn/Ni/MnCID-5CG were obtained.

Scanning Transmission Electron Microscope Observation. An ethanol dispersion of the powder samples was dropped onto a carbon grid and allowed to dry by standing at room temperature. STEM-EDX measurements were conducted using a JEOL JEM-2200 TEM under an operating voltage of 200 kV.

Synchrotron Powder X-ray Diffraction Measurement and Analysis. Powder samples of each compound were sealed in silica glass capillaries. XRPD patterns with good count statistics were measured using synchrotron radiation employing a large Debye–Scherrer camera with imaging plate detectors on the BL02B2 beamline at the Super Photon Ring (SPring-8) facility in Japan. All the XRPD patterns were obtained using a step size of $2\theta = 0.01^\circ$. The powder patterns were indexed using the DICVOL91 indexing software package. The unit cell parameters were refined using the Le Bail fitting method employing the Rietica software package.

Other Physical Measurements. The adsorption isotherms of MeOH at 298 K were conducted using a BELSORP-18. Thermogravimetric analysis (TGA) was conducted using a Rigaku Thermo plus TG 8120 TGA apparatus at a heating rate of 10 K/min. Inductively coupled plasma (ICP) analysis was conducted after the degradation of the crystals had occurred in HNO₃ using a Shimadzu ICPE-9000 spectrometer.

Time-Course Analysis of the Crystal Formation Kinetics of Powder Crystals. Time-course analysis of the crystal formation kinetics was conducted as follows. Addition of the metal perchlorate precursors to a DMF/MeOH solution of the ligand precursors at 70 °C was determined as the starting point ($t = 0$) of the experiments. The crystals were filtered, washed with MeOH, and then dried under vacuum at 150 °C. The sample weight of the crystals was measured. The yield of the crystals was calculated by measuring the sample weight of crystals collected at each reaction time. The ratio of metal ions was determined from ICP analysis and X-ray fluorescence data of the mixed metal compounds.

Determination of the Induction Time (t_{ind}). The induction time (t_{ind}) was defined as the time required for powder formation from the reaction solution. In the experiment, t_{ind} was determined from visual inspection of the solution which corresponds to the onset of turbidity.

■ ASSOCIATED CONTENT

● Supporting Information

Tables of the crystal parameters for MnCID-5CG, elemental analysis, and contents of Mn in both solid-solution and phase-separated type $[\text{Zn}_{1-x}\text{Mn}_x(\text{NO}_2\text{-ip})(\text{bpy})]_n$. Figures include XRD spectra, TGA profiles, photographs of the reaction process, time-course analyses of crystal formation, LeBail fitting analysis results, SEM images, STEM-EDX images, EDX spectra, and adsorption isotherms. This material is available free of charge via the Internet at <http://pubs.acs.org>.

■ AUTHOR INFORMATION

Corresponding Author

kitagawa@icems.kyoto-u.ac.jp

Notes

The authors declare no competing financial interest.

■ ACKNOWLEDGMENTS

The authors thank Mr. Ryohei Numaguchi, Dr. Hayato Sugiyama, Ms. Ai Yamamoto, Dr. Hideki Tanaka, Dr. Satoshi Watanabe, and Prof. Minoru Miyahara for fruitful discussions on the gate-opening behavior of flexible compounds. This work was supported by the Japan Science and Technology Agency (JST) PRESTO program, Grants-in-Aid for Scientific Research, Japan Society for the Promotion of Science (JSPS), the WPI-iCeMS program, and the JST ERATO program. iCeMS is supported by the World Premier International Research Initiative (WPI), MEXT, Japan. T.F. is grateful to the JSPS Research Fellowship for Young Scientists.

■ REFERENCES

- (1) (a) Jones, C. W.; Tsuji, K.; Davis, M. E. *Nature* **1998**, *393*, 52. (b) Kuznicki, S. M.; Bell, V. A.; Nair, S.; Hillhouse, H. W.; Jacobinas, R. M.; Braunbarth, C. M.; Toby, B. H.; Tsapatsis, M. *Nature* **2001**, *412*, 720. (c) Chmiola, J.; Yushin, G.; Gogotsi, Y.; Portet, C.; Simon, P.; Taberna, P. L. *Science* **2006**, *313*, 1760.
- (2) (a) Yang, C. N.; Lee, T. D. *Phys. Rev.* **1952**, *87*, 404. (b) Lee, T. D.; Yang, C. N. *Phys. Rev.* **1952**, *87*, 410. (c) Laughlin, R. B.; Pines, D.; Schmalian, J.; Stojkovic, B. P.; Wolyne, P. *Proc. Natl. Acad. Sci. U.S.A.* **2000**, *97*, 32.
- (3) (a) Hehn, M.; Ounadjela, K.; Bucher, J. P.; Rousseaux, F.; Decanini, D.; Bartenlian, B.; Chappert, C. *Science* **1996**, *272*, 1782. (b) Park, J. I.; Cheon, J. *J. Am. Chem. Soc.* **2001**, *123*, 5743.

- (4) Maier, J. *Nat. Mater.* **2005**, *4*, 805.
- (5) (a) Arndt, M.; Stannarius, R.; Groothues, H.; Hempel, E.; Kremer, F. *Phys. Rev. Lett.* **1997**, *79*, 2077. (b) Kahn, O.; Martinez, C. *J. Science* **1998**, *279*, 44.
- (6) (a) Yaghi, O. M.; O'Keeffe, M.; Ockwig, N. W.; Chae, H. K.; Eddaoudi, M.; Kim, J. *Nature* **2003**, *423*, 705. (b) Das, S.; Kim, H.; Kim, K. *J. Am. Chem. Soc.* **2009**, *131*, 3814. (c) Tanabe, K. K.; Cohen, S. M. *Chem. Soc. Rev.* **2011**, *40*, 498. (d) Stock, N.; Biswas, S. *Chem. Rev.* **2012**, *112*, 933.
- (7) (a) Robson, R. *J. Chem. Soc. Dalton Trans.* **2000**, 3735. (b) Kitagawa, S.; Kitaura, R.; Noro, S. *Angew. Chem., Int. Ed.* **2004**, *43*, 2334. (c) Ferey, G.; Mellot-Draznieks, C.; Serre, C.; Millange, F. *Acc. Chem. Res.* **2005**, *38*, 217.
- (8) Burrows, A. D. *CrystEngComm* **2011**, *13*, 3623.
- (9) (a) Chun, H.; Dybtsev, D. N.; Kim, H.; Kim, K. *Chem.—Eur. J.* **2005**, *11*, 3521. (b) Kleist, W.; Jutz, F.; Maciejewski, M.; Baiker, A. *Eur. J. Inorg. Chem.* **2009**, 3552. (c) Deng, H. X.; Doonan, C. J.; Furukawa, H.; Ferreira, R. B.; Towne, J.; Knobler, C. B.; Wang, B.; Yaghi, O. M. *Science* **2010**, *327*, 846. (d) Fukushima, T.; Horike, S.; Inubushi, Y.; Nakagawa, K.; Kubota, Y.; Takata, M.; Kitagawa, S. *Angew. Chem., Int. Ed.* **2010**, *49*, 4820.
- (10) (a) Furukawa, S.; Hirai, K.; Nakagawa, K.; Takashima, Y.; Matsuda, R.; Tsuruoka, T.; Kondo, M.; Haruki, R.; Tanaka, D.; Sakamoto, H.; Shimomura, S.; Sakata, O.; Kitagawa, S. *Angew. Chem., Int. Ed.* **2009**, *48*, 1766. (b) Furukawa, S.; Hirai, K.; Takashima, Y.; Nakagawa, K.; Kondo, M.; Tsuruoka, T.; Sakata, O.; Kitagawa, S. *Chem. Commun.* **2009**, 5097. (c) Koh, K.; Wong-Foy, A. G.; Matzger, A. J. *Chem. Commun.* **2009**, 6162.
- (11) (a) Khan, N. A.; Haque, M. M.; Jhung, S. H. *Eur. J. Inorg. Chem.* **2010**, 4975. (b) Haque, E.; Jeong, J. H.; Jhung, S. H. *CrystEngComm* **2010**, *12*, 2749. (c) Kang, I. J.; Khan, N. A.; Haque, E.; Jhung, S. H. *Chem.—Eur. J.* **2011**, *17*, 6437. (d) Haque, E.; Jhung, S. H. *Chem. Eng. J.* **2011**, *173*, 866. (e) Haque, E.; Khan, N. A.; Kim, C. M.; Jhung, S. H. *Cryst. Growth. Des.* **2011**, *11*, 4413.
- (12) (a) Horike, S.; Tanaka, D.; Nakagawa, K.; Kitagawa, S. *Chem. Commun.* **2007**, 3395. (b) Tanaka, D.; Nakagawa, K.; Higuchi, M.; Horike, S.; Kubota, Y.; Kobayashi, L. C.; Takata, M.; Kitagawa, S. *Angew. Chem., Int. Ed.* **2008**, *47*, 3914. (c) Nakagawa, K.; Tanaka, D.; Horike, S.; Shimomura, S.; Higuchi, M.; Kitagawa, S. *Chem. Commun.* **2010**, *46*, 4258. (d) Sato, H.; Matsuda, R.; Sugimoto, K.; Takata, M.; Kitagawa, S. *Nat. Mater.* **2010**, *9*, 661. (e) Tanaka, D.; Henke, A.; Albrecht, K.; Moeller, M.; Nakagawa, K.; Kitagawa, S.; Groll, J. *Nat. Chem.* **2010**, *2*, 410. (f) Hijikata, Y.; Horike, S.; Sugimoto, M.; Sato, H.; Matsuda, R.; Kitagawa, S. *Chem.—Eur. J.* **2011**, *17*, 5137. (g) Hijikata, Y.; Horike, S.; Tanaka, D.; Groll, J.; Mizuno, M.; Kim, J.; Takata, M.; Kitagawa, S. *Chem. Commun.* **2011**, *47*, 7632. (h) Takashima, Y.; Furukawa, S.; Kitagawa, S. *CrystEngComm* **2011**, *13*, 3360. (i) Kishida, K.; Horike, S.; Nakagawa, K.; Kitagawa, S. *Chem. Lett.* **2012**, *41*, 425. (j) Horike, S.; Inubushi, Y.; Hori, T.; Fukushima, T.; Kitagawa, S. *Chem. Sci.* **2012**, *3*, 116.
- (13) Livage, C.; Forster, P. M.; Guillou, N.; Tafaya, M. M.; Cheetham, A. K.; Ferey, G. *Angew. Chem., Int. Ed.* **2007**, *46*, 5877.
- (14) (a) Weissbuch, I.; Addadi, L.; Lahav, M.; Leiserowitz, L. *Science* **1991**, *253*, 637. (b) Leff, D. V.; Ohara, P. C.; Heath, J. R.; Gelbart, W. M. *J. Phys. Chem.* **1995**, *99*, 7036. (c) Lacmann, R.; Herden, A.; Mayer, C. *Chem. Eng. Technol.* **1999**, *22*, 279. (d) Uemura, T.; Hoshino, Y.; Kitagawa, S.; Yoshida, K.; Isoda, S. *Chem. Mater.* **2006**, *18*, 992. (e) Tsuruoka, T.; Furukawa, S.; Takashima, Y.; Yoshida, K.; Isoda, S.; Kitagawa, S. *Angew. Chem., Int. Ed.* **2009**, *48*, 4739. (f) Zacher, D.; Liu, J. N.; Huber, K.; Fischer, R. A. *Chem. Commun.* **2009**, 1031. (g) Vekilov, P. G. *Cryst. Growth Des.* **2010**, *10*, 5007. (h) Carreon, M. A.; Venna, S. R.; Jasinski, J. B. *J. Am. Chem. Soc.* **2010**, *132*, 18030. (i) Cravillon, J.; Schroder, C. A.; Nayuk, R.; Gummel, J.; Huber, K.; Wiebcke, M. *Angew. Chem., Int. Ed.* **2011**, *50*, 8067. (j) Falcaro, P.; Hill, A. J.; Nairn, K. M.; Jasieniak, J.; Mardel, J. I.; Bastow, T. J.; Mayo, S. C.; Gimona, M.; Gomez, D.; Whitfield, H. J.; Ricco, R.; Patelli, A.; Marmiroli, B.; Amenitsch, H.; Colson, T.; Villanova, L.; Buso, D. *Nat. Commun.* **2011**, *2*. (k) Nayuk, R.; Zacher, D.; Schweins, R.; Wiktor, C.;

Fischer, R. A.; van Tendeloo, G.; Huber, K. *J. Phys. Chem. C* **2012**, *116*, 6127.

(15) (a) Diring, S.; Furukawa, S.; Takashima, Y.; Tsuruoka, T.; Kitagawa, S. *Chem. Mater.* **2010**, *22*, 4531. (b) Huber, K.; Cravillon, J.; Nayuk, R.; Springer, S.; Feldhoff, A.; Wiebcke, M. *Chem. Mater.* **2011**, *23*, 2130. (c) Guo, H. L.; Zhu, Y. Z.; Wang, S.; Su, S. Q.; Zhou, L.; Zhang, H. J. *Chem. Mater.* **2012**, *24*, 444.

(16) Denton, A. R.; Ashcroft, N. W. *Phys. Rev. A* **1991**, *43*, 3161.

(17) Toshima, N.; Yonezawa, T.; Kushihashi, K. *J. Chem. Soc., Faraday. Trans.* **1993**, *89*, 2537.

(18) Horike, S.; Shimomura, S.; Kitagawa, S. *Nat. Chem.* **2009**, *1*, 695.

(19) (a) Li, D.; Kaneko, K. *Chem. Phys. Lett.* **2001**, *335*, 50.

(b) Kitaura, R.; Seki, K.; Akiyama, G.; Kitagawa, S. *Angew. Chem., Int. Ed.* **2003**, *42*, 428.

(20) (a) Coudert, F. X.; Jeffroy, M.; Fuchs, A. H.; Boutin, A.; Mellot-Draznieks, C. *J. Am. Chem. Soc.* **2008**, *130*, 14294. (b) Watanabe, S.; Sugiyama, H.; Adachi, H.; Tanaka, H.; Miyahara, M. T. *J. Chem. Phys.* **2009**, *130*. (c) Coudert, F. X.; Boutin, A.; Jeffroy, M.; Mellot-Draznieks, C.; Fuchs, A. H. *ChemPhysChem* **2011**, *12*, 247.

(21) (a) Kanoh, H.; Kondo, A.; Noguchi, H.; Kajiro, H.; Tohdoh, A.; Hattori, Y.; Xu, W. C.; Moue, M.; Sugiura, T.; Morita, K.; Tanaka, H.; Ohba, T.; Kaneko, K. *J. Colloid Interface Sci.* **2009**, *334*, 1. (b) Rabone, J.; Yue, Y. F.; Chong, S. Y.; Stylianou, K. C.; Bacsá, J.; Bradshaw, D.; Darling, G. R.; Berry, N. G.; Khimyak, Y. Z.; Ganin, A. Y.; Wiper, P.; Claridge, J. B.; Rosseinsky, M. J. *Science* **2010**, *329*, 1053.

(22) Triguero, C.; Coudert, F. X.; Boutin, A.; Fuchs, A. H.; Neimark, A. V. *J. Phys. Chem. Lett.* **2011**, *2*, 2033.

(23) The value of 16 kPa for methanol vapor pressure corresponds to 0.95 in relative pressure (P/P_s) at 25 °C. The uptake at this pressure region can be regarded as saturation state in the vapor adsorption.

(24) The gate-opening pressure (P_{go}) was estimated from the inflection point of the sigmoidal adsorption curve.

(25) Liu, X. W.; Hu, J.; Pan, B. C. *Physica E* **2008**, *40*, 3042.